Materials & Design 213 (2022) 110342

Contents lists available at ScienceDirect

Materials & Design

journal homepage:

Numerical study of the aggregate contact effect on the complex modulus of asphalt concrete

Zhifei Tan [a], Zhen Leng [a,*], Jiwang Jiang [a], Peng Cao [b], Denis Jelagin [c], Gaoyang Li [a], Anand Sreeram [d]

[a] Department of Civil and Environmental Engineering, The Hong Kong Polytechnic University, Hung Hom, Kowloon, Hong Kong
[b] College of Architecture and Civil Engineering, Beijing University of Technology, Beijing, China
[c] Department of Civil and Architectural Engineering, KTH Royal Institute of Technology, Brinellvägen 23, 10044 Stockholm, Sweden
[d] Department of Civil, Architectural and Environmental Engineering, The University of Texas at Austin, Austin, TX, USA

HIGHLIGHTS

- 3D numerical models of asphalt concrete containing aggregate contact zones were developed.
- The steady-state dynamic method effectively predicted the complex modulus of an asphalt concrete numerical model with millions of elements.
- Despite its very small volumetric percentage, contact zone can significantly improve the stress transmission between aggregates in asphalt concrete.
- Considering contact zone can significantly increase the predicted moduli of asphalt concrete at low frequencies and overall prediction accuracy.

GRAPHICAL ABSTRACT

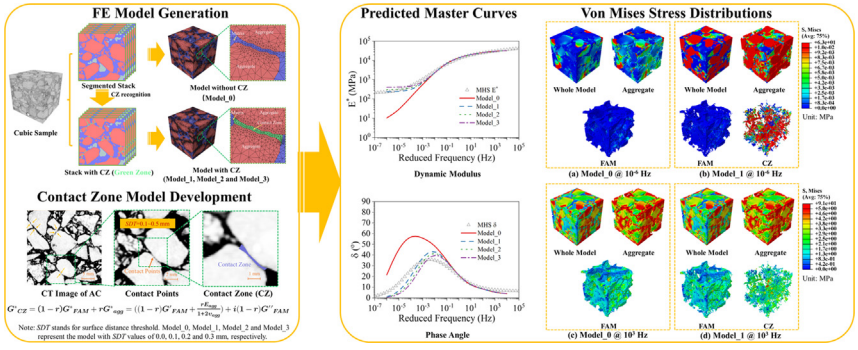

ARTICLE INFO

Article history:
Received 4 June 2021
Revised 20 September 2021
Accepted 20 December 2021
Available online 21 December 2021

Keywords:
Complex modulus
Aggregate contacts
Steady-state dynamics
Finite element analysis

ABSTRACT

Asphalt concrete (AC) is a composite material consisting of binder, aggregates and air voids. The quantitative effect of aggregate-to-aggregate contact on the mechanical performance of AC is an important and complex issue, which has not been fully understood yet. To fill this gap, this study aims to characterize the aggregate contacts in AC and evaluate their effects on the viscoelastic behavior of AC through micromechanical finite element (FE) modeling. To this end, 3D microstructural models were generated through digital image processing (DIP) method and aggregate contacts were captured in the model via contact zone (CZ) elements. A CZ model was proposed and verified by a parametric study to identify the viscoelastic properties of CZ elements, while the viscoelastic properties of matrix phase were determined through laboratory tests. Steady-state dynamic (SSD) analysis was then conducted to investigate the macro-scale viscoelastic response of AC. It was found that the proposed modeling approach captures the measured response accurately. Accounting for aggregate contacts results in higher predicted AC dynamic moduli and lower phase angles, thus improving the agreement between modeling and experimental results. The numerical model developed in this study provides a promising approach for investigating the effect of aggregate contacts on the mechanical performance of AC.

* Corresponding author.
E-mail address: zhen.leng@polyu.edu.hk (Z. Leng).

https://doi.org/10.1016/j.matdes.2021.110342

1. Introduction

As asphalt concrete (AC) is a heterogeneous composite material with a high-volume proportion of aggregates, its mechanical properties are significantly influenced by the aggregate skeleton. Previous studies showed that aggregate skeleton plays a dominant role in the rutting and cracking resistance, and dynamic performance of AC [1–4]. The aggregate skeleton has been commonly characterized by aggregate spatial distributions, aggregate orientations, packing, and aggregate contact characteristics [5–7]. In particular, aggregate contact characteristics define the interaction of the adjacent aggregate particles and thus play an important role in the load transmission in AC [8,9]. The contact properties are affected by the aggregate morphology, such as aggregate angularity and surface texture [10,11]. It has been reported in many studies that aggregate contacts significantly affect the mechanical behavior of AC, such as rutting resistance and viscoelastic properties. The rutting resistance performance was characterized by evaluating the internal structure of AC before and after cyclic mechanical loading. It was found that AC with more aggregate contacts shows better rutting performance [3–5]. The effect of aggregate contacts on the viscoelastic properties of AC has been discussed in studies on micromechanical FE modeling of AC, as it is usually found that the analytical and numerical models significantly underestimate the stiffness of asphalt materials, especially at high temperatures (low frequencies) [1,12–15]. It has been hypothesized that this underestimation could be attributed to the lack of consideration of the aggregate contacts in the model [16–18]. However, further studies on the effects of aggregate contacts on the mechanical performance of AC are limited, although such aggregate contacts have been more deeply studied in other research areas, such as powder compaction [19–21].

Recently, a few studies attempted to use modeling methods to characterize the effect of aggregate contacts on the viscoelastic properties of AC. Some incorporated aggregate contacts into the analytical micromechanical models and found an improvement in the accuracy of the predicted viscoelastic performance of AC [22–24]. However, since the analytical micromechanical models cannot take the detailed microstructure of AC into account, their accuracy with respect to capturing aggregate contacts is quite limited [23]. Besides, discrete element method (DEM) has been used in several studies to investigate the effect of aggregate contacts on AC performance [25,26]. DEM is advantageous in situations where the material response is fully controlled by contact interactions, such as in the case of loose asphalt mixtures [27,28]. At the same time, as DEM is based on discrete particles, it cannot fully capture the complicated rheological behavior of the binder phase. Arshadi and Bahia applied the 2D finite element (FE) model to evaluate the aggregate contact effect on the creep deformation [29]. However, to fully capture the mechanical response of AC, a 3D FE model considering aggregate contacts is required [1]. Therefore, an approach to effectively incorporate the aggregate contacts into the 3D numerical micromechanical modeling of AC is still lacking. The objective of the present study is to alleviate this shortcoming.

One of the possible methods to introduce the aggregate contacts into modeling is the digital image processing (DIP) method, which allows the construction of a 3D model based on X-ray CT images [30]. Although the precise aggregate contacts in the matrix between two adjacent aggregates are hardly captured on 2D X-ray CT images, the narrow areas between the adjacent aggregates, so-called contact zones (CZ), can be identified and quantified [31,32]. However, incorporating aggregate contacts into the model may be problematic in terms of the meshing and computational time. Due to the complicated microstructures of AC, an insufficiently fine mesh may not accurately capture the thin CZ and compromise the model accuracy [33–35], while refining the mesh further will make the computation significantly more demanding and sometimes impossible [36].

Accordingly, this study aims to develop a numerical micromechanical model which is capable of capturing the effect of aggregate contacts on AC response in a computationally efficient manner. An approach to generate 3D numerical models with and without aggregate contacts was proposed. The aggregate contacts in AC were quantified through X-Ray CT measurements on AC cores and incorporated into the numerical model. Frequency sweep tests were conducted on the fine aggregate matrix (FAM), the mix of fine aggregate and asphalt binder, to characterize its viscoelastic properties, which were used as the matrix properties in the numerical model. To include the contacts among coarse aggregate particles into the numerical models, CZ elements were incorporated between the adjacent aggregate particles with their viscoelastic properties identified through a parametric study by combining the experimental viscoelasticity of FAM and elasticity of aggregates. Finally, an efficient FE modeling method based on steady-state dynamic (SSD) was adopted to evaluate the resulting macro-scale viscoelastic properties of AC. The obtained modeling results are compared with the measurements from the frequency sweep tests.

2. Microstructural modeling of AC

AC is commonly visualized as a three-phase material consisting of a viscoelastic binder matrix, elastic aggregates, and air voids. In this study, two types of 3D microstructural models of AC were developed. An AC model not accounting for aggregate contacts was composed of aggregate, matrix, and air void phases, while an additional CZ phase was introduced in the model with aggregate contacts.

To generate the microstructural models for FE simulation, the different phases of AC were identified from X-ray CT data through DIP. Fig. 1 illustrates the procedure for the DIP in this study. Firstly, a small cubic sample with a length of 20 mm was extracted out from the X-ray CT images with a resolution of 0.098 mm. After that, the segmentation method proposed by Onifade et al. was applied to segment the FAM matrix, aggregate (>2.36 mm), and air void phases [37]. It is worth noting that because the algorithms cannot automatically separate all aggregates, the processed images should be further manually treated to improve the segmentation quality.

To develop the model with CZ, the first step is to identify the CZ regions from the CT images. Surface distance threshold (*SDT*), which defines the distance between surfaces of contacting aggregates, is commonly used to characterize the CZ in AC. However, there is still no consensus on selecting the *SDT* value, which may be affected by the aggregate surface texture. Research has indicated that the texture depth of aggregate surface is smaller than 0.5 mm [32]. Considering the resolution of images (0.098 mm), three *SDT* values, including 0.1 mm, 0.2 mm, and 0.3 mm, were adopted to define the CZ in the microstructural models with aggregate contacts. A MATLAB program was developed to find out the CZ phase based on the defined *SDT* values from the segmented 2D image stacks [38,39]. By reconstructing the segmented 2D image stacks, four 3D microstructural models, including one model without CZ and three models with CZ (corresponding to *SDT* = 0.1, 0.2, and 0.3 mm), were developed and labeled as Model_0, Model_1, Model_2, and Model_3, respectively. Table 1 presents the volume compositions of the real AC specimen and the developed models, which show good consistency. It is worth noting that the CZ phases only occupy small volume percentages of AC, which are smaller than 12% in all models with CZ.

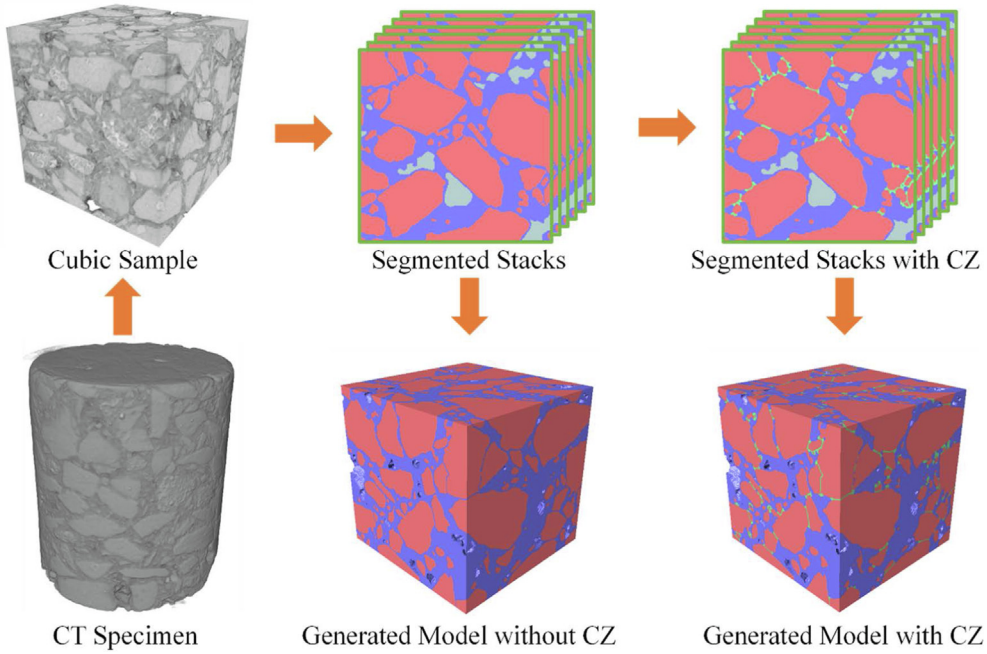

Fig. 1. Digital image processing. CZ represents contact zone.

Table 1
The volume percentage of each phase in the real AC and developed models (%).

Sample ID	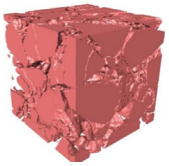 Aggregate	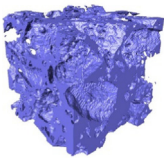 Matrix	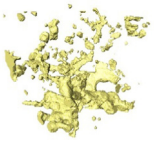 Air Void	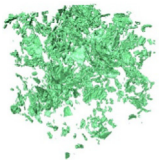 Contact Zone
CT Specimen	63.5	32.0	4.5	–
Model_0	63.5	31.6	4.9	–
Model_1	63.8	29.4	4.9	1.9
Model_2	64.0	25.5	4.9	5.6
Model_3	64.0	20.0	4.8	11.2

Note: Model_0, Model_1, Model_2 and Model_3 represent the model with *SDT* values of 0, 0.1, 0.2 and 0.3 mm, respectively.

The FE mesh was generated in this study using the advanced Delaunay-based mesh method, which is commonly used to mesh the complex 2D and 3D structures [40]. To ensure the mesh quality, special attention should be paid to two issues. First, the mesh should be constrained to the generated surface of different phases since the generated elements may interpolate into the area of other phases and cause the artificial merging at the proximity zone of aggregates. Second, a finer mesh size should be applied to the CZ phase in order not to distort CZ volume. In this study, the linear tetrahedral element (C3D4) with an average size of 0.98 mm was used to mesh the bulk of the models, and the mesh in the CZ phases was further densified by the elements with an average size of 0.049 mm. Mesh sensitivity analysis on other mesh sizes was conducted, verifying the suitability of the selected mesh parameters. Fig. 2 presents the meshed models of Model_0 and Model_1. The element numbers for the four models were 1.89 million, 6.26 million, 6.91 million, and 7.36 million, respectively.

3. Experimental study

To obtain input parameters for the AC model presented in the previous section and validate it, viscoelastic properties of one type of AC mixture were measured along with the properties of the corresponding FAM. The measurements were performed through frequency sweep tests. Tests on FAM were used to determine the viscoelastic properties of the matrix phase in the numerical model. The master curves measured for the mixture were used to evaluate the model's accuracy. In this study, an AC (SMA10) commonly used in Hong Kong was selected, which is a gap-graded stone matrix asphalt mixture with a nominal maximum aggregate size of 10 mm. The fine aggregate particles smaller than 2.36 mm, mineral filler, and asphalt binder were considered as the composition of FAM. The method proposed by Underwood and Kim was adopted to determine the compositions of FAM in this study [41]. Table 2 presents the gradations of the asphalt mixture and FAM. The

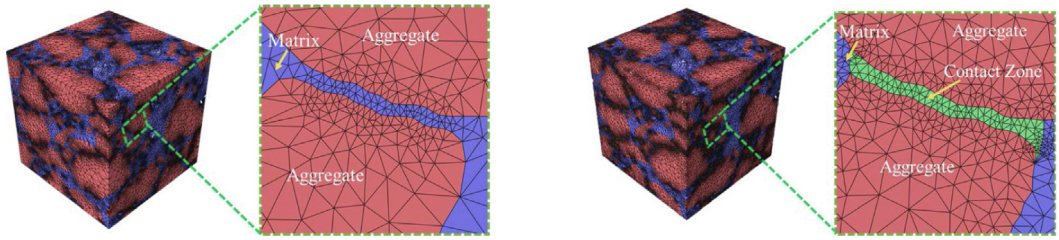

Fig. 2. Meshed models: (a) model without CZ and (b) Model with 0.1 mm CZ.

Table 2
Gradations of AC and FAM.

Sieve size (mm)	SMA10	FAM
	Passing percentage (%)	Passing percentage (%)
14	100.0	–
10	96.0	–
5	27.0	–
2.36	22.0	100.0
1.18	19.0	84.9
0.6	18.0	79.9
0.3	16.0	69.8
0.15	14.2	60.7
0.075	12.9	54.2
Binder Content (%)	6.0	21.1

asphalt binder with a Superpave performance grade of PG76-16 and granite mineral filler and aggregates were used to prepare the FAM and AC specimens. Frequency sweep tests were conducted using a dynamic shear rheometer (DSR) and a universal testing machine (UTM) to measure the viscoelastic properties of FAM and AC, respectively, as shown in Fig. 3 [42,43]. All tests were conducted at the strain levels below the linear viscoelastic limit.

After the frequency sweep tests, the Williams-Landel-Ferry (WLF) equation [44] and the Arrhenius equation were used to shift the frequency sweep data for FAM and AC at different temperatures to the reference temperature of 10 °C, respectively. Then, the shifted data were smoothened by the modified Huet-Sayegh (MHS) model proposed by Woldekidan et al. [45], which can capture the complex modulus of FAM and mixture over a wide frequency range. The constructed complex modulus master curves for the FAM and mixture are presented in Fig. 4.

To incorporate the viscoelastic properties into FE simulation, the master curves of FAM fitted by the MHS model were further expressed in the format of the Prony series. Fig. 5 displays the constructed master curves of FAM fitted by the Prony series model and the corresponding fitted parameters are presented in Table 3. It can be seen that the Prony series model can capture both the dynamic shear modulus and phase angle master curves well within the whole frequency range from 10^{-6} Hz to 10^{5} Hz.

4. Contact zone characterization

In the developed microstructural model of AC, the effect of aggregate contacts on the viscoelastic response of AC was captured by incorporating additional material phase, i.e., contact zone (CZ) material. The constitutive and geometrical properties of CZ may have a significant influence on the modeling outcomes. In this section, the proposed CZ model is first described in detail, followed by the CZ model verification through numerical study.

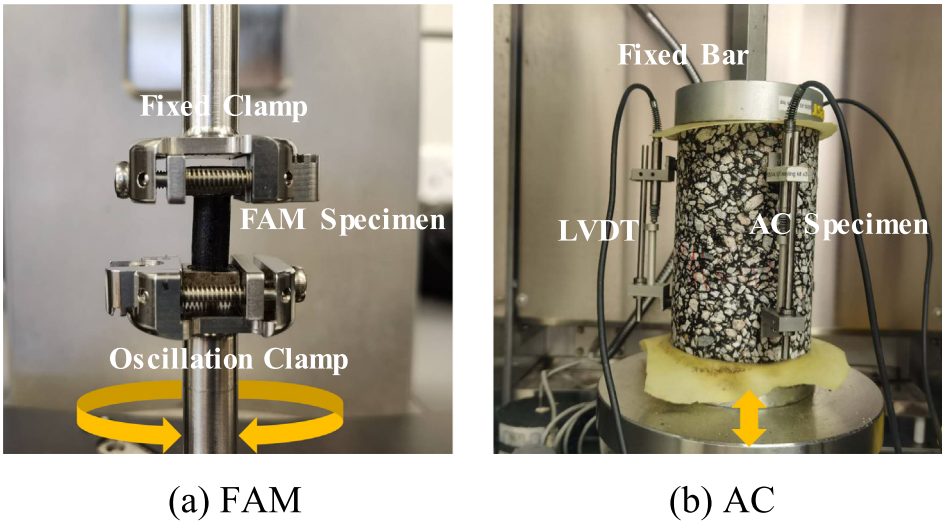

Fig. 3. Measuring systems for (a) FAM and (b) AC.

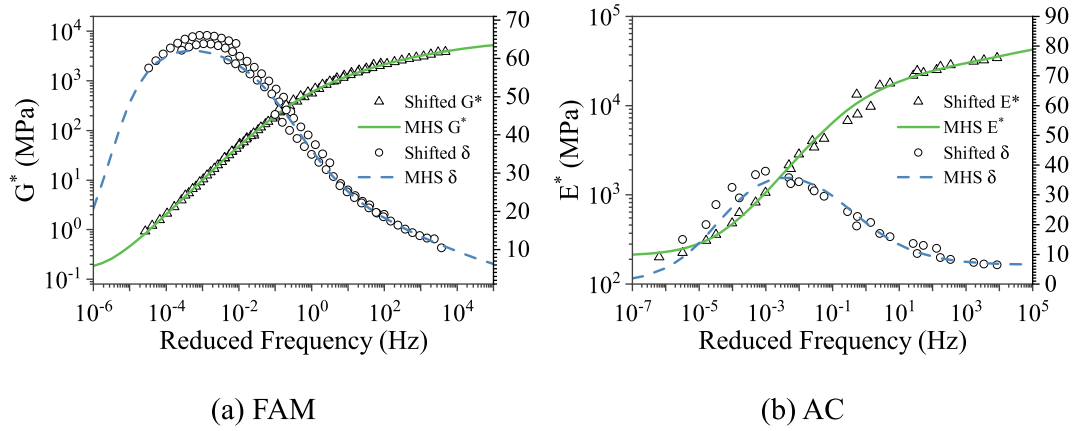

Fig. 4. Constructed complex modulus master curves for (a) FAM and (b) AC. The shifted points and the MHS curves represent the shifted experimental data points and the constructed master curve by the MHS model.

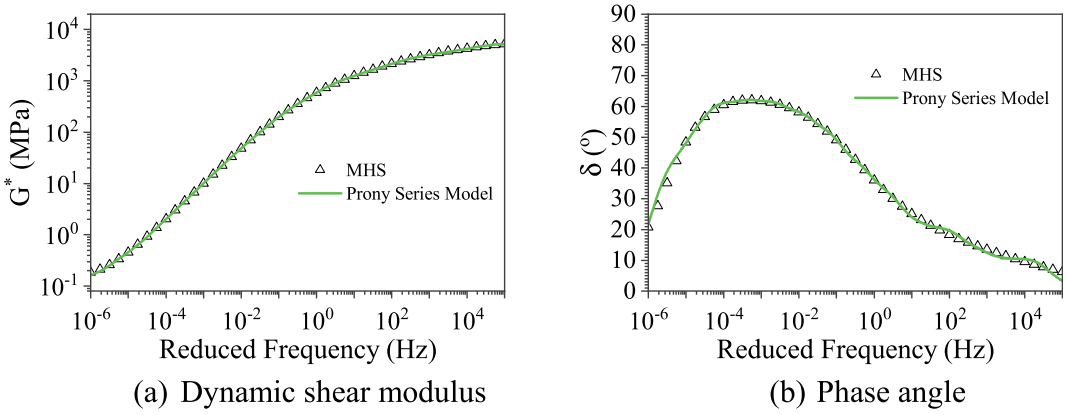

Fig. 5. Comparison of the developed master curves by fitted Prony series model with the experimental master curves developed by MHS model.

Table 3
Material properties.

Materials	Bulk density	Poisson's ratio	Elasticity/Viscoelasticity
Aggregate	2.65	0.2	60,000 MPa
FAM	2.00	0.4	Prony Series Model
Contact zone	2.00	0.4	Prony Series Model

Prony Series Parameters

	FAM		CZ (r = 25/60,000)		CZ (r = 50/60,000)		CZ (r = 100/60,000)	
G_0 (MPa)	5,249		5,328		5,337		5,275	
Series No.	τ_i	α_i	τ_i	α_i	τ_i	α_i	τ_i	α_i
1	7.35E−06	2.41E−01	7.35E−06	2.43E−01	7.35E−06	2.43E−01	9.57E−06	2.62E−01
2	4.08E−05	1.17E−01	4.08E−05	1.07E−01	4.08E−05	1.07E−01	6.91E−05	1.45E−01
3	2.26E−04	1.44E−01	2.26E−04	1.79E−01	2.26E−04	1.79E−01	4.98E−04	1.91E−01
4	1.25E−03	1.83E−01	1.25E−03	1.36E−01	1.25E−03	1.35E−01	3.60E−03	1.48E−01
5	6.95E−03	9.64E−02	6.95E−03	1.26E−01	6.95E−03	1.26E−01	2.60E−02	1.23E−01
6	3.85E−02	1.12E−01	3.85E−02	9.76E−02	3.85E−02	9.74E−02	1.87E−01	8.03E−02
7	2.14E−01	6.37E−02	2.14E−01	6.66E−02	2.14E−01	6.65E−02	1.35E + 00	3.21E−02
8	1.19E + 00	3.10E−02	1.19E + 00	2.98E−02	1.19E + 00	2.98E−02	9.76E + 00	8.10E−03
9	6.57E + 00	9.31E−03	6.57E + 00	9.27E−03	6.57E + 00	9.25E−03	7.04E + 01	1.82E−03
10	3.64E + 01	2.66E−03	3.64E + 01	2.62E−03	3.64E + 01	2.61E−03	5.08E + 02	4.48E−04
11	2.02E + 02	7.08E−04	2.02E + 02	7.07E−04	2.02E + 02	7.05E−04	3.67E + 03	8.85E−05
12	1.12E + 03	2.24E−04	1.12E + 03	2.21E−04	1.12E + 03	2.21E−04	2.65E + 04	3.28E−05
13	6.21E + 03	4.62E−05	6.21E + 03	4.88E−05	6.21E + 03	4.86E−05		
14	3.44E + 04	2.82E−05	3.44E + 04	2.47E−05	3.44E + 04	2.47E−05		

Notes: G_0 is initial shear modulus, $\tau_i$is relaxation time, and α_i is weight.

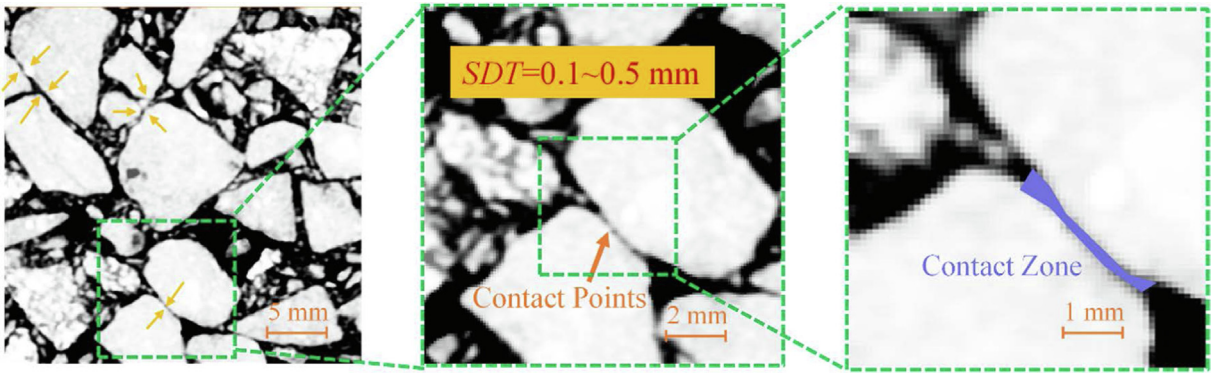

Fig. 6. Aggregate contacts in AC. *SDT* stands for surface distance threshold.

4.1. Contact zone model

To illustrate the concept of CZ, the 2D internal structure of AC is presented in Fig. 6. In the CT images, it can be observed that the neighboring aggregates contact each other through contact points. Since the precise contact points in the matrix between two adjacent aggregates are hardly captured on the 2D X-ray CT images, *SDT*, which defines the maximum surface distance between the neighboring aggregates' perimeters, has been adopted to consider the aggregate contacts in AC [31,32]. Accordingly, CZ, which refers to the narrow area captured by *SDT*, is defined to consider the aggregate contacts in AC [31,32].

In the narrow CZ, the neighboring aggregates contact each other via the contact points and gaps between them are filled with FAM. As aggregate is considered as an elastic material, while the FAM is a viscoelastic material, the properties of CZ may be assumed to be influenced by both the viscoelasticity of the matrix and the elasticity of aggregates. Accordingly, a parameter r was introduced in this study, which represents the contribution percentage of aggregate modulus to the CZ modulus, while the contribution of the FAM's modulus is $(1-r)$. Correspondingly, the following equations were used to calculate the complex shear modulus of CZ:

$$G^*_{FAM} = G'_{FAM} + iG''_{FAM} \tag{1}$$

$$G^*_{agg} = G'_{agg} + iG''_{agg} = \frac{E_{agg}}{(1+2\upsilon_{agg})} + 0i \tag{2}$$

$$\begin{aligned} \text{So, } G^*_{CZ} &= (1-r)G^*_{FAM} + rG^*_{agg} \\ &= \left((1-r)G'_{FAM} + \frac{rE_{agg}}{1+2\upsilon_{agg}}\right) + i(1-r)G''_{FAM} \end{aligned} \tag{3}$$

where FAM, agg and CZ refer to fine aggregate matrix, aggregate, and contact zone; G^*, G' and G'' represent the complex shear modulus, storage modulus, and loss modulus of the corresponding materials. υ_{agg} represents the Poisson's ratio of aggregate, which is equal to 0.2.

Fig. 7 presents the complex modulus master curves of the CZ with different r values. r values are expressed as the ratio of the Young's modulus of aggregates (60,000 MPa) as the reference. In total, four r values were evaluated, including 0, 10/60,000, 100/60,000 and 1,000/60,000. As expected, with the increasing r, the properties of CZ transform from the viscoelastic FAM to elastic aggregate with the rising dynamic moduli but decreasing phase angles.

4.2. Contact zone model verification

To verify the reliability of the proposed material model, the 2D CZ numerical models with simplified microstructures were developed as displayed in Fig. 8. The top and bottom green layers represent the adjacent aggregates, the white zone in the center represents the matrix in CZ between the two aggregates, and the triangles represent the contact points in the CZ. The number of contact points is highly correlated to the surface characteristics of aggregates. The difference in the volume content of triangles (v) represents different contact point fractions between aggregates. The sandwich model represents the completely smooth interface between aggregates, which is equivalent to the CZ in the model without contact. Dynamic simulations were performed on the developed CZ model as described in Section 5. Fig. 9 presents the predicted master curves. It can be noticed that the triangular models offer significantly higher stiffness than the sandwich model by showing larger dynamic moduli and smaller phase angles, especially within the low-frequency range. This result verifies the assumption that the surface irregularities of aggregate can improve the stiffness of CZ. However, with the increase of frequency, the predicted master curves of both dynamic modulus and phase angle from different models converged, indicating that the effect of the microstructure of CZ is diminished with the increasing frequency. Besides, comparing Fig. 9 with Fig. 7, it can be seen that with the increase of r values of the proposed CZ model, the master curves present the same trend as the predicted master curves with the increase of triangular volume, which indicates that the r value in the proposed model can be correlated to the contact points in CZ. The high agreement of the predicted master curves from the proposed model and developed CZ microstructural model also suggested that the proposed CZ model in Section 4.1 can capture the change of the viscoelastic CZ with frequencies. Thus, this proposed model can be used to model the dynamic performance of AC, where the sample suffers a very small vertical deformation. However, considering that the real contacts in the AC are much complicated, the model may not be applicable under other complex boundary conditions.

5. Computational study

In the modeling conducted, the aggregate was considered as a linear-elastic material, while the FAM and CZ were considered as linear-viscoelastic materials. The viscoelastic properties of FAM and CZ were expressed in the format of the Prony series models. All the Prony series models can well capture the viscoelastic properties within the full frequency range, ensuring the accuracy of

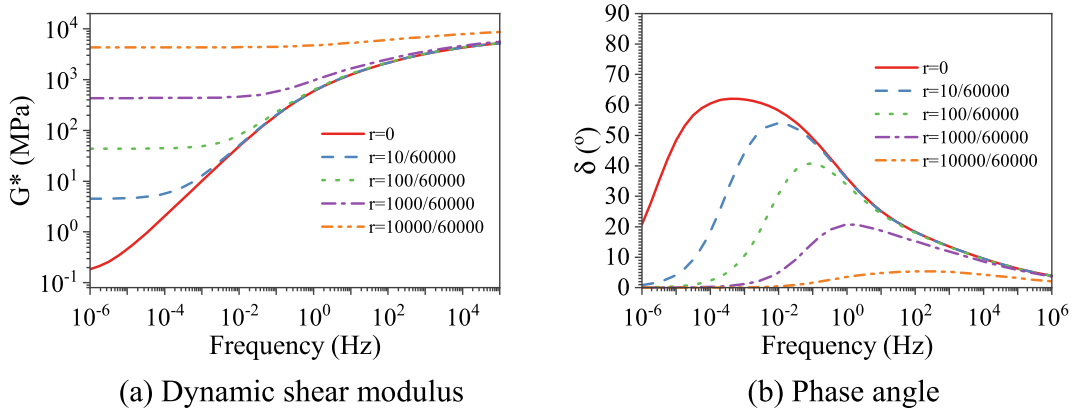

Fig. 7. Predicted master curves of CZ by the proposed CZ model at different *r* values.

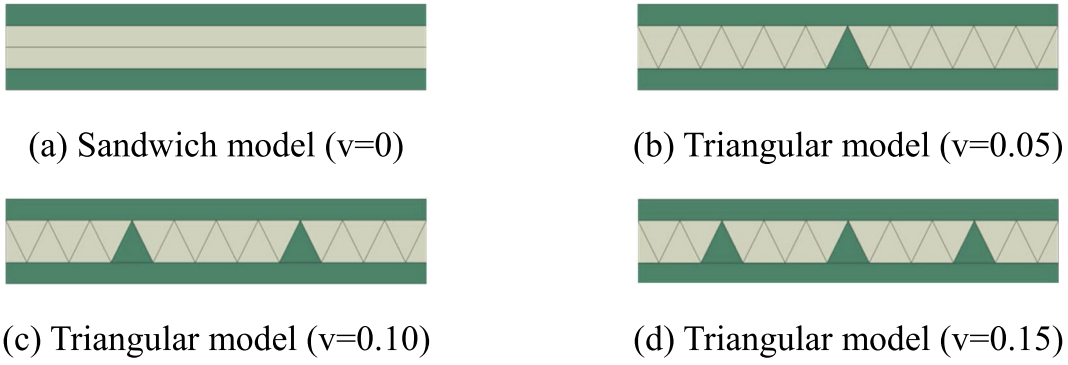

Fig. 8. Simplified CZ microstructural models with different triangular volume contents. The top and bottom green layers represent the adjacent aggregates, the white zone in the center represents the matrix in CZ between the two aggregates, and the triangles represent the contact points in the CZ.

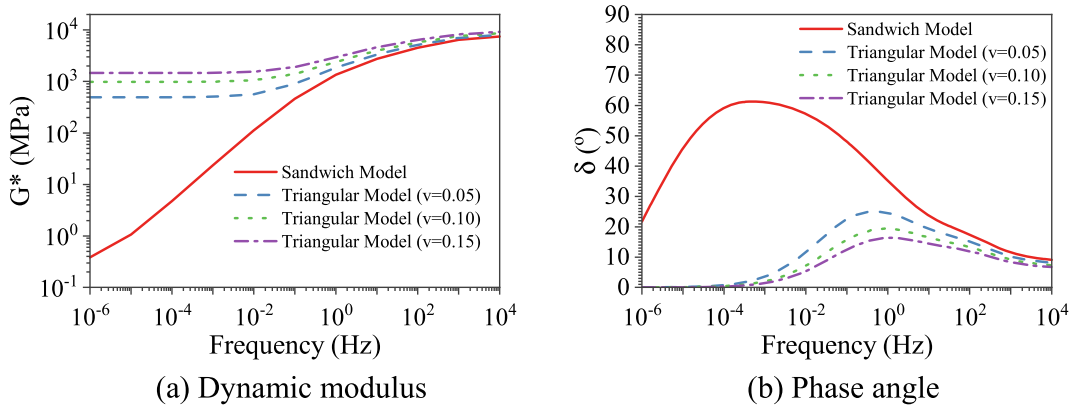

Fig. 9. Predicted master curves of CZ by simplified CZ microstructural models.

modeling results. A subroutine was applied to input the Prony series models into the ABAQUS software. The material properties for the three components in AC are presented in Table 3. To analyze the effect of the modulus of CZ on the viscoelastic performance of AC, three different *r* values, including 25/60,000, 50/60,000, and 100/60,000, were selected based on the long-term modulus of AC from the MHS model. The three *r* values representing aggregate contribution on CZ are 25 MPa, 50 MPa, and 100 MPa, respectively.

To conduct the FE simulation, a vertical loading was applied at the top surface of the numerical model and the bottom surface was fixed. Then, the SSD analysis was performed to obtain the complex moduli within the frequency range of 10^{-6} Hz to 10^{4} Hz. SSD analysis procedure is a perturbation procedure [46] and this procedure

is conducted as a frequency sweep by applying the loads at a series of different frequencies [47]. Therefore, the complex moduli at different frequencies can be directly obtained by one simulation. A computer with a 2.8 GHz Intel® Xeon® Processors E5-2680 v2 was used, and it took no more than 3 h to compute 11 frequency points within the modeling frequency range for all the 3D models.

6. Results

6.1. Effect of contact zones on the complex modulus

To evaluate the effect of CZ on the dynamic response of AC, two parameters including *SDT* and *r* were assessed. *SDT* determines the content of CZ in the AC, while *r* determines the material properties of CZ. The models with three different *SDT* values were evaluated. Fig. 10 presents the predicted master curves of the four models at the *r* value of 25/60,000. It can be observed that for the three models with CZ, increasing *SDT* values slightly improves the predicted modulus at low frequencies by showing higher dynamic moduli but lower phase angles. A threshold value of 0.1 mm is capable of improving the simulated modulus to the level of the experimental values. Thus, it is believed that the *SDT* value of 0.1 mm can cover almost all the CZ. The further increase of *SDT* values only incorporates more matrices as CZ and cannot significantly affect the dynamic performance of AC. Therefore, Model_1 with an *SDT* value equal to 0.1 mm was used in the following analysis.

Besides, Fig. 10 also reveals the effects of CZ on the viscoelastic behavior of AC. By comparing the master curves of Model_0, the model without contact, with other models in Fig. 10 (a) and (b), it can be found that CZ can significantly improve the prediction of complex moduli within the low-frequency range by showing higher moduli and lower phase angles. In contrast, the model without CZ (Model_0) substantially underestimates the moduli of AC within the low-frequency range. However, the effect of aggregate contacts decreases with the frequency increase. The predicted master curves of dynamic modulus and phase angle converge with experimental curves when the frequency is higher than 0.1 Hz, which indicates that the aggregate contact mainly affects the dynamic response of AC at relatively low frequencies. The reason could be that with the increase of frequency, the stiffened FAM diminishes the effect of contact on the performance of AC. Fig. 10 (c) and (d) present the master curves of storage modulus and loss modulus, which show that CZ mainly increases the storage moduli but has no significant effect on the loss moduli within the low-frequency range. This is because, within the low-frequency range, CZ is more like an elastic material. Compared with the experimental curves, the predicted master curves show smaller loss moduli at low frequencies. It may be caused by the underestimation of the modulus of FAM in the laboratory test. Factors such as air void in the FAM specimen may decrease the measured modulus of FAM.

The relationship between the viscoelastic properties of CZ on the complex modulus of AC is presented in Fig. 11. It can be observed that with increasing *r*, the dynamic moduli increase and phase angles decrease within the low-frequency range. This is due to the aggregate contact that can stiffen AC at low frequencies. Therefore, a higher *r* value gives the AC a higher modulus. Besides, a *r* value of 25/60,000, which is equivalent to a contribution of the aggregate of 25 MPa, gives better predictions of

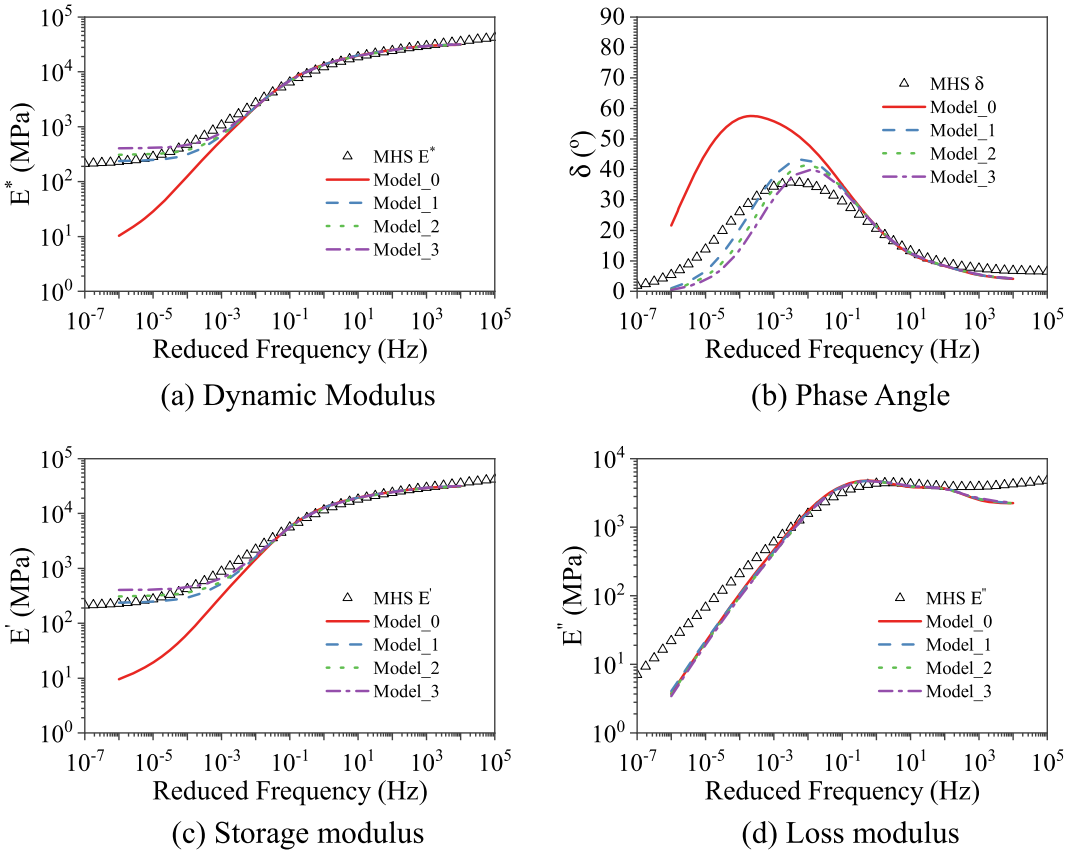

Fig. 10. Predicted master curves based on 3D numerical models with different *SDT* values. Model_0, Model_1, Model_2 and Model_3 represent the numerical models with 0.0 mm, 0.1 mm, 0.2 mm, and 0.3 mm *SDT* values, respectively.

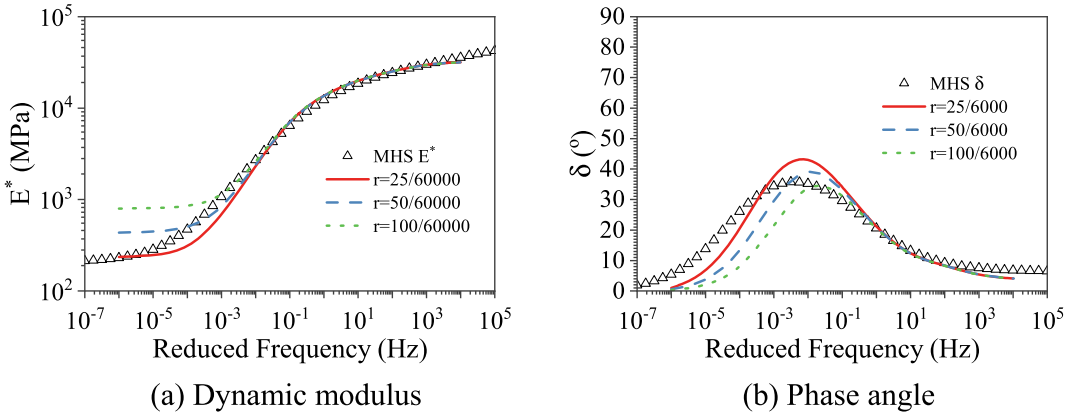

Fig. 11. Predicted master curves based on the numerical model at different *r* values. MHS curves represent the experimental master curves developed by the MHS model.

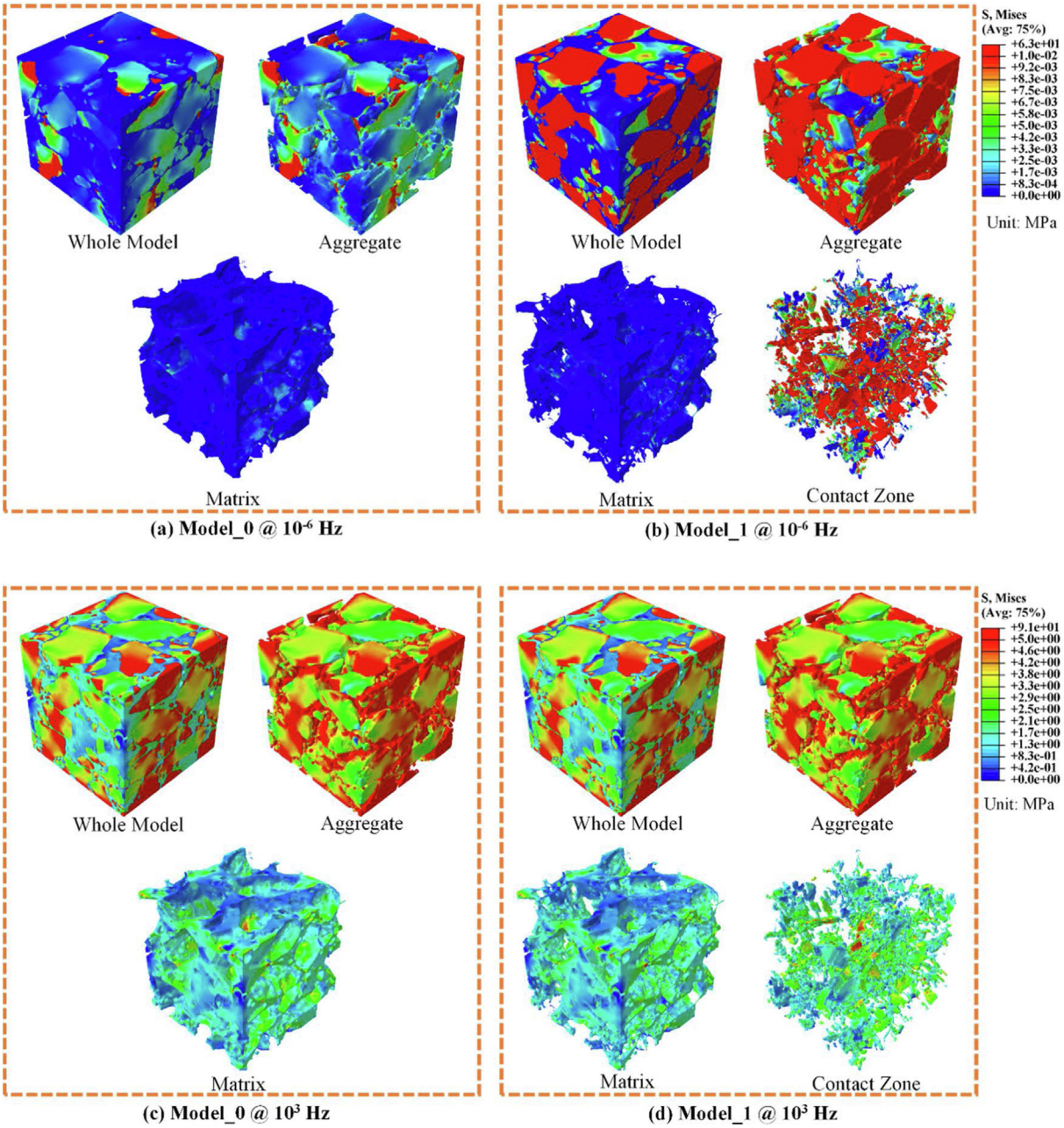

Fig. 12. Von Mises stress distributions in model without CZ (Model_0) and model with CZ (Model_1) at 10^{-6} Hz and 10^{3} Hz.

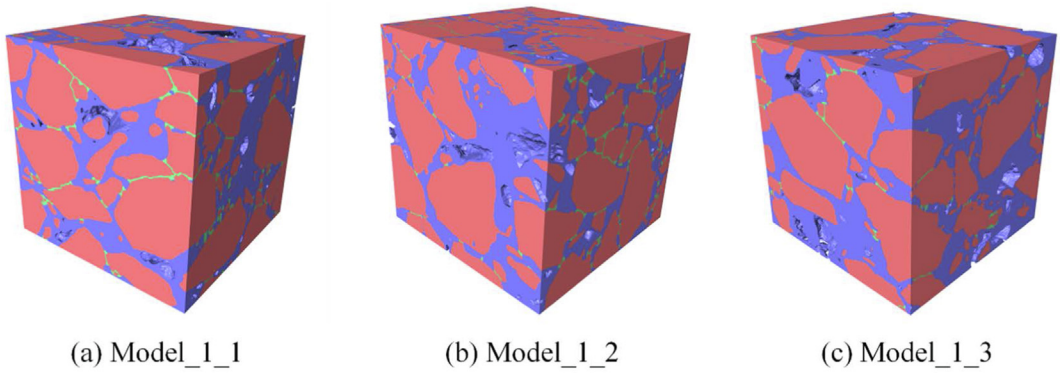

Fig. 13. Constructed three different microstructural models with 0.1 mm *SDT* value.

Table 4
The volume percentages of the developed three different models (%).

Model ID	Aggregate	Matrix	Air void	Contact zone
Model_1_1	63.8	29.4	4.9	1.9
Model_1_2	69.1	26.3	1.4	3.1
Model_1_3	58.2	32.0	8.3	1.5

dynamic moduli and phase angles than the other two *r* values, which indicates that this value is more suitable for the aggregate used in this study. It is worth noting that the performance of AC is highly affected by the modulus at low frequency. For example, the modulus at the frequency of 10^{-6} Hz corresponds to the modulus of AC at 50 °C and 0.01 Hz. This scenario commonly happens in actual pavements, for example, when the vehicle is waiting for the traffic light at the intersection in summer. If the modulus of AC is too small, the pavement may be susceptible to rutting.

6.2. Stress distributions in asphalt concrete

To further understand how aggregate contacts affect the internal response of AC at different loading frequencies, the von Mises stress distributions of the models without and with CZ were further analyzed. Fig. 12 presents the stress distributions of each phase in Model_0 and Model_1 at a low frequency of 10^{-6} Hz and a high frequency of 10^{3} Hz.

Fig. 12 (a) and (b) present the stress distributions at the low frequency of 10^{-6} Hz. It can be clearly observed that the aggregate phase in Model_1 shows much higher stress than Model_0, which indicates a better stress transmission among aggregates in Model_1. This can be attributed to the CZ in Model_1. It can be found that in Model_1, CZ also shows much higher stress than FAM, indicating that CZ can improve the efficiency of load transmission among aggregates, although it only occupies a tiny percentage (1.9% in this study) in AC. Furthermore, the high stress concentration at the perimeters of close aggregates also indicates the importance of CZ in load transmission. Thus, it can be concluded that CZ plays a vital role in the mechanical performance of AC at low frequencies. Different from the low frequency, from Fig. 12 (c) and (d), it can be found that at the high frequency of 10^{3} Hz, the stress distributions in both models are almost identical and all phases in AC display very high stress, which indicates that the stiffened FAM with the increase of frequency can improve the stress transmission in AC. Thus, the effect of CZ on the dynamic response of AC is diminished. This result is consistent with the assumption that the impact of microstructural properties on the mechanical performance of AC decreases with the increase of frequency.

7. Discussion

To evaluate the effects of the microstructural variability on the dynamic response of AC, two more models were generated as

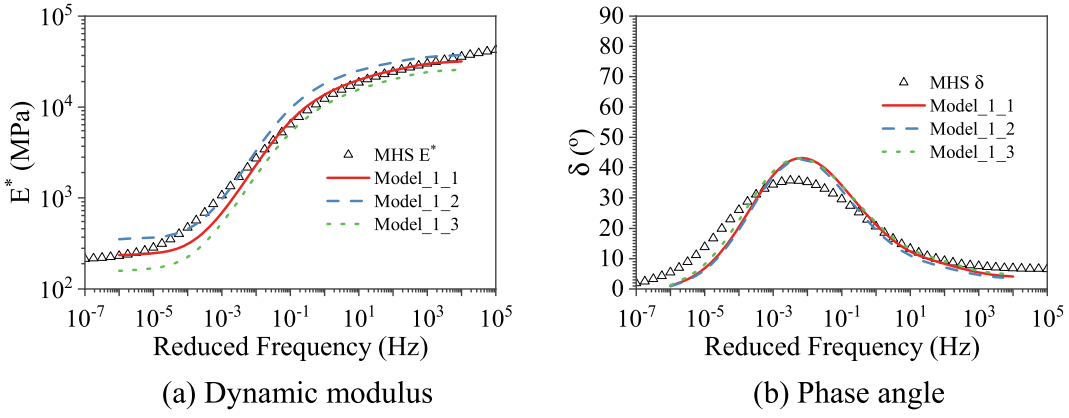

Fig. 14. Predicted master curves based on the developed three microstructural models with 0.1 mm *SDT* value.

shown in Fig. 13. To simplify, the three models with an *SDT* value of 0.1 mm were labeled as Model_1_1, Model_1_2, and Model_1_3, accordingly. Since the three models were extracted from different places of the CT specimen, their microstructures and compositions were different, as presented in Fig. 13 and Table 4. Model_1_2 has the highest aggregate content, followed by Model_1_1 and Model_1_3. Their predicted master curves of dynamic modulus and phase angle are presented in Fig. 14. It can be seen that the model with higher aggregate volume content shows higher dynamic moduli within the whole frequency range. It is reasonable since more aggregates may make AC stiffer. However, the three models present almost identical phase angle master curves, which indicated that the increase in aggregate volume content only improves the elastic performance of AC but cannot influence the viscous performance of AC. Moreover, it can be observed that although the microstructures of the three models are different, all the predicted master curves are reasonable.

8. Conclusions

In this study, a new micromechanical FE modeling approach was proposed. In order to account for the effect of aggregate-to-aggregate contacts on the AC macro-scale performance, a contact zone (CZ) approach was developed. Optimal modeling parameters of CZ were identified from the parametric study and the model was used to evaluate the effect of aggregate contacts on the viscoelastic properties of AC. Based on the outcomes of this study, the following conclusions can be drawn:

(1) Although CZ only occupies a tiny volume percentage in AC, it can significantly increase the moduli of AC within the low-frequency range due to its much higher modulus than asphalt matrix. It has been found that CZ only occupied 1.9% volume in AC. By comparing the predicted master curves of the model without CZ (Model_0), a significant improvement in the complex moduli of the model with CZ (Model_1) at low frequencies has been observed.
(2) As the contact medium between aggregates, CZ can significantly improve the accuracy of load transmission in AC at low loading frequencies. The stress distributions in the model at 10^{-6} Hz show that the CZ phase has much higher stress than the matrix phase, indicating CZ plays a critical role in the load transmission between aggregates.
(3) The proposed micromechanical FE model by integrating digital image processing and SSD method provides an accurate and efficient approach to predict the dynamic response of AC. The developed micromechanical FE model can well capture the CZ in AC. Besides, for the FE model with millions of elements, the dynamic simulation based on the SSD method can be completed in several hours, indicating the efficiency of the proposed SSD method.

It can be concluded that the method proposed in this study is effective in incorporating aggregate contact characteristics in the prediction of the complex modulus of AC. In future studies, the effect of aggregate contacts on other mechanical properties of AC, such as rutting resistance, creep, and fatigue resistance, will be further explored.

Declaration of Competing Interest

The authors declare that they have no known competing financial interests or personal relationships that could have appeared to influence the work reported in this paper.

Acknowledgments

This study is sponsored by the Hong Kong Research Grant Council General Research Fund (Project Number: 15209920), the Innovation and Technology Fund - Guangdong-Hong Kong Technology Cooperation Funding Scheme (GHP/116/18GD), and the Hong Kong Asphalt (Green) Limited (PolyU Project ID P0036391). We would like to thank K. Wah Asphalt Limited in Hong Kong for providing the experimental materials.

References

[1] F.T. Aragão, Y. Kim, P. Karki, D.N. Little, Semiempirical, analytical, and computational predictions of dynamic modulus of asphalt concrete mixtures, Transp. Res. Rec. 2181 (1) (2010) 19–27.
[2] F. Moreno, M. Rubio, Effect of aggregate nature on the fatigue-cracking behavior of asphalt mixes, Mater. Des. 47 (2013) 61–67.
[3] L.T. Souza, Y.-R. Kim, F.V. Souza, L.S. Castro, Experimental testing and finite-element modeling to evaluate the effects of aggregate angularity on bituminous mixture performance, J. Mater. Civ. Eng. 24 (3) (2012) 249–258.
[4] Y.-R. Kim, H.M. Park, F.T.S. Aragão, J.E.S. Lutif, Effects of aggregate structure on hot-mix asphalt rutting performance in low traffic volume local pavements, Constr. Build. Mater. 23 (6) (2009) 2177–2182.
[5] E. Masad, M.E. Kutay, Characterization of the internal structure of asphalt mixtures, Transportation Research E-Circular EC161, Transportation Research Board, Washington, DC, 2012, pp. 2–16.
[6] S. Saadeh, L. Tashman, E. Masad, W. Mogawer, Spatial and directional distribution of aggregates in asphalt mixes, J. Test. Eval. 30 (6) (2002) 483–491.
[7] D.M. Kusumawardani, Y.D. Wong, Evaluation of aggregate gradation on aggregate packing in porous asphalt mixture (PAM) by 3D numerical modelling and laboratory measurements, Constr. Build. Mater. 246 (2020) 118414.
[8] H. Zhu, J.E. Nodes, Contact based analysis of asphalt pavement with the effect of aggregate angularity, Mech. Mater. 32 (3) (2000) 193–202.
[9] C. Jin, X. Wan, X. Yang, P. Liu, M. Oeser, Three-dimensional characterization and evaluation of aggregate skeleton of asphalt mixture based on force-chain analysis, J. Eng. Mech. 147 (2) (2021) 04020147.
[10] T. Pan, E. Tutumluer, S.H. Carpenter, Effect of coarse aggregate morphology on permanent deformation behavior of hot mix asphalt, J. Transp. Eng. 132 (7) (2006) 580–589.
[11] J. Gao, H. Wang, Y. Bu, Z. You, M.R.M. Hasan, M. Irfan, Effects of coarse aggregate angularity on the microstructure of asphalt mixture, Constr. Build. Mater. 183 (2018) 472–484.
[12] X. Shu, B. Huang, Dynamic modulus prediction of HMA mixtures based on the viscoelastic micromechanical model, J. Mater. Civ. Eng. 20 (8) (2008) 530–538.
[13] B.S. Underwood, Y.R. Kim, Effect of volumetric factors on the mechanical behavior of asphalt fine aggregate matrix and the relationship to asphalt mixture properties, Constr. Build. Mater. 49 (2013) 672–681.
[14] J. Chen, H. Wang, H. Dan, Y. Xie, Random modeling of three-dimensional heterogeneous microstructure of asphalt concrete for mechanical analysis, J. Eng. Mech. 144 (9) (2018) 04018083.
[15] P. Karki, Y.-R. Kim, D.N. Little, Dynamic modulus prediction of asphalt concrete mixtures through computational micromechanics, Transp. Res. Rec. 2507 (1) (2015) 1–9.
[16] B.S. Underwood, Y.R. Kim, A four phase micro-mechanical model for asphalt mastic modulus, Mech. Mater. 75 (2014) 13–33.
[17] W.G. Buttlar, D. Bozkurt, G.G. Al-Khateeb, A.S. Waldhoff, Understanding asphalt mastic behavior through micromechanics, Transp. Res. Rec. 1681 (1) (1999) 157–169.
[18] C. El Sawda, F. Fakhari-Tehrani, J. Absi, F. Allou, C. Petit, Multiscale heterogeneous numerical simulation of asphalt mixture, Mater. Des. Process. Commun. 1 (3) (2019) e42.
[19] F.T.S. Aragão, D.A. Hartmann, A.R.G. Pazos, Y.-R. Kim, Virtual fabrication and computational simulation of asphalt concrete microstructure, Int. J. Pavement Eng. 18 (9) (2017) 859–870.
[20] A. Khoei, S. Biabanaki, A. Vafa, S. Taheri-Mousavi, A new computational algorithm for 3D contact modeling of large plastic deformation in powder forming processes, Comput. Mater. Sci. 46 (1) (2009) 203–220.
[21] R. Ransing, D. Gethin, A. Khoei, P. Mosbah, R. Lewis, Powder compaction modelling via the discrete and finite element method, Mater. Des. 21 (4) (2000) 263–269.
[22] H. Zhang, K. Anupam, A. Scarpas, C. Kasbergen, S. Erkens, Effect of stone-on-stone contact on porous asphalt mixes: Micromechanical analysis, Int. J. Pavement Eng. 21 (8) (2020) 990–1001.
[23] H. Zhang, K. Anupam, T. Scarpas, C. Kasbergen, S. Erkens, L. Al Khateeb, Continuum-based micromechanical models for asphalt materials: Current practices & beyond, Constr. Build. Mater. 260 (2020) 119675.
[24] Y. Sun, J. Chen, B. Pan, X. Shu, B. Huang, Three-dimensional micromechanical complex-modulus prediction of asphalt concrete considering the aggregate interlocking effect, J. Mater. Civ. Eng. 29 (10) (2017) 04017153.

[25] E. Olsson, D. Jelagin, M.N. Partl, New discrete element framework for modelling asphalt compaction, Road Mater. Pavement Des. 20 (sup2) (2019) S604–S616.
[26] X. Yang, Z. You, C. Jin, A. Diab, M.R. Mohd Hasan, Aggregate morphology and internal structure for asphalt concrete: prestep of computer-generated microstructural models, Int. J. Geomech. 18 (10) (2018) 06018024.
[27] F. Chen, D. Jelagin, M.N. Partl, Vibration-induced aggregate segregation in asphalt mixtures, Mater. Struct. 53 (2) (2020) 1–14.
[28] F. Chen, D. Jelagin, M.N. Partl, Experimental and numerical analysis of asphalt flow in a slump test, Road Mater. Pavement Des. 20 (sup1) (2019) S446–S461.
[29] C. Ling, A. Arshadi, H. Bahia, Importance of binder modification type and aggregate structure on rutting resistance of asphalt mixtures using image-based multi-scale modelling, Road Mater. Pavement Des. 18 (4) (2017) 785–799.
[30] X. Yang, Z. You, Z. Wang, Q. Dai, Review on heterogeneous model reconstruction of stone-based composites in numerical simulation, Constr. Build. Mater. 117 (2016) 229–243.
[31] A.R. Coenen, M.E. Kutay, N.R. Sefidmazgi, H.U. Bahia, Aggregate structure characterisation of asphalt mixtures using two-dimensional image analysis, Road Mater. Pavement Des. 13 (3) (2012) 433–454.
[32] M.E. Kutay, E. Arambula, N. Gibson, J. Youtcheff, Three-dimensional image processing methods to identify and characterise aggregates in compacted asphalt mixtures, Int. J. Pavement Eng. 11 (6) (2010) 511–528.
[33] Q. Dai, K. Ng, 2D cohesive zone modeling of crack development in cementitious digital samples with microstructure characterization, Constr. Build. Mater. 54 (2014) 584–595.
[34] Y. Zhao, J. Jiang, L. Zhou, F. Ni, Improving the calculation accuracy of FEM for asphalt mixtures in simulation of SCB test considering the mesostructure characteristics, Int. J. Pavement Eng. (2020) 1–15.
[35] A. Arshadi, H. Bahia, Development of an image-based multi-scale finite-element approach to predict mechanical response of asphalt mixtures, Road Mater. Pavement Des. 16 (sup2) (2015) 214–229.
[36] P. Cao, F. Jin, Z. Changjun, D. Feng, Investigation on statistical characteristics of asphalt concrete dynamic moduli with random aggregate distribution model, Constr. Build. Mater. 148 (2017) 723–733.
[37] I. Onifade, D. Jelagin, A. Guarin, B. Birgisson, N. Kringos, Asphalt Internal Structure Characterization with X-Ray Computed Tomography and Digital Image Processing, Springer, Netherlands, Dordrecht, 2013, pp. 139–158.
[38] J. Jiang, F. Ni, L. Gao, L. Yao, Effect of the contact structure characteristics on rutting performance in asphalt mixtures using 2D imaging analysis, Constr. Build. Mater. 136 (2017) 426–435.
[39] J. Jiang, F. Ni, Q. Dong, L. Yao, X. Ma, Investigation of the internal structure change of two-layer asphalt mixtures during the wheel tracking test based on 2D image analysis, Constr. Build. Mater. 209 (2019) 66–76.
[40] H. Si, TetGen, a Delaunay-based quality tetrahedral mesh generator, ACM Trans. Math. Software (TOMS) 41 (2) (2015) 1–36.
[41] B.S. Underwood, Y.R. Kim, Microstructural investigation of asphalt concrete for performing multiscale experimental studies, Int. J. Pavement Eng. 14 (5) (2013) 498–516.
[42] Y. Zhang, Z. Leng, Quantification of bituminous mortar ageing and its application in ravelling evaluation of porous asphalt wearing courses, Mater. Des. 119 (2017) 1–11.
[43] R.M. Huurman, L. Mo, M.F. Woldekidan, Unravelling porous asphalt concrete towards a mechanistic material design tool, Road Mater. Pavement Des. 11 (3) (2010) 583–612.
[44] D.A. Anderson, D.W. Christensen, H. Bahia, Physical properties of asphalt cement and the development of performance-related specifications, J. Assoc. Asphalt Paving Technol. 60 (1991).
[45] M. Woldekidan, M. Huurman, A. Pronk, A modified HS model: Numerical applications in modeling the response of bituminous materials, Finite Elem. Anal. Des. 53 (2012) 37–47.
[46] ABAQUS, ABAQUS 6.14 analysis user's manual, Dassault Systems Inc Waltham, USA, 2014..
[47] P. Cao, F. Jin, C. Zhou, D. Feng, W. Song, Steady-state dynamic method: An efficient and effective way to predict dynamic modulus of asphalt concrete, Constr. Build. Mater. 111 (2016) 54–62.